# Assembling quantum dots via critical Casimir forces

Marino, E.; Kodger, T.E.; Hove, J.B. ten; Velders, A.H.; Schall, P.

[Link to publication](Link to publication)

**Citation for published version (APA):**
Marino, E., Kodger, T. E., Hove, J. B. T., Velders, A. H., & Schall, P. (2016). Assembling quantum dots via critical Casimir forces. *Solar Energy Materials and Solar Cells*, *158*(2), 154-159. https://doi.org/10.1016/j.solmat.2016.01.016

# Assembling quantum dots via critical Casimir forces

Emanuele Marino [a], Thomas E. Kodger [a], Jan Bart ten Hove [b], Aldrik H. Velders [b], Peter Schall [a,*]

[a] *Van der Waals – Zeeman Institute, Universiteit van Amsterdam, Science Park 904, 1098 XH Amsterdam, The Netherlands*
[b] *Department of BioNanoTechnology, Wageningen Universiteit, Dreijenplein 6, 6700EK Wageningen, The Netherlands*

A B S T R A C T

Programmed assembly of colloidal inorganic nanocrystal superstructures is crucial for the realization of future artificial solids as well as present optoelectronic applications. Here, we present a new way to assemble quantum dots reversibly using binary solvents. By tuning the temperature and composition of the binary solvent mixture, we achieve reversible aggregation of nanocrystals in solution induced by critical Casimir forces. We study the temperature-sensitive quantum-dot assembly with dynamic light scattering. We show that careful screening of the electrostatic repulsion by adding salt provides a further parameter to tune the reversible assembly.

© 2016 The Authors. Published by Elsevier B.V. This is an open access article under the CC BY license (http://creativecommons.org/licenses/by/4.0/).

## 1. Introduction

Semiconductor nanocrystals, *quantum dots* (QDs), offer the unique possibility for controlling optical and electronic properties by simply tuning their size. The act of confining electronic excitations within linear dimensions smaller than the bulk exciton Bohr radius gives rise to quantum effects leading to the discretization of the band structure and to a size-dependent bandgap. While it has been possible to characterize the properties of single (non-interacting) dots, recently considerable effort has been made in the pursuit of well-ordered superstructures, the goal being to understand the collective effects therein [1–5]. Indeed, successfully exploiting inter-dot coupling would improve electronic transport throughout QD-based solar cells, therefore increasing power conversion efficiency values in such devices. To achieve charge transport, charges need to "hop" from one QD to another; however, this process is slow and not very efficient, since multiple recombination events may occur. Nevertheless, both simulations and experiments have shown that efficient inter-dot coupling is possible and could improve charge extraction efficiency [6–10].

A promising route is through the formation of delocalized molecular orbital-like states that extend over multiple dots; in this case, charges can travel by more efficient coherent resonant tunneling. Yet, achieving this regime of transport requires careful assembly of a very monodisperse QD dispersion [11]. Combining

precise synthesis techniques with assembly of colloidal QDs into structures would yield bottom-up tailored material properties, while showing the beneficial transport characteristics of bulk semiconductors [12,13].

In this letter, we report temperature-dependent assembly of QDs via critical Casimir forces. We use a binary solvent close to its critical point; in such critical solvents, solvent concentration fluctuations arise and, being confined between two QDs surfaces, yield to an attractive force that induces assembly. We use dynamic light scattering to follow growing QD aggregates with time. By subtlety tuning the composition of the mixture, salt content and temperature, we grow aggregates reversibly with direct temperature control. The assembly of colloidal particles with size smaller than the length scale of solvent fluctuations has never previously been investigated; this regime is often addressed in the literature as the *protein limit* and we hereby present the very first experimental work in this regard [14]. The results shown offer new opportunities in the assembly of nanostructures.

## 2. Principles of aggregation

Binary solvents consisting of a liquid mixture with typically an aqueous and an apolar, 3-methylpyridine (3MP), component provide new opportunities for quantum-dot assembly. They allow solvent-mediated interactions to be exploited, which have recently attracted increasing interest in the field of colloidal science [15]. A typical solvent phase diagram is shown in Fig. 1, in which solvent phases are indicated as a function of composition and temperature.
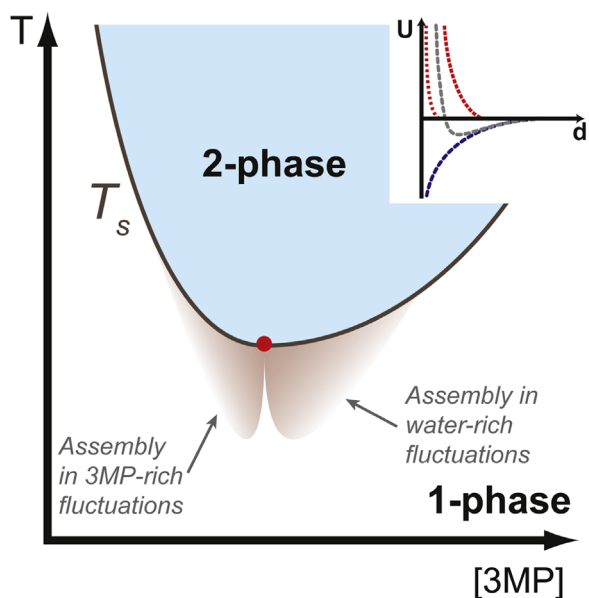
**Fig. 1.** Schematic phase diagram of the binary solvent. The phase separation temperature, $T_s$, varies as a function of the concentration of 3-methylpyridine, [3MP]; for $T > T_s$ the mixture features two phases (blue-shaded area), while for $T < T_s$ it appears homogeneous. The critical point coincides with the minimum value of $T_s$ (red point). In the proximity of the critical point, solvent concentration fluctuations arise (red-shaded area); on the left side of the critical point they are 3MP-rich, while on the right side they are water-rich. Inset: Behavior of attractive Casimir (blue line) and repulsive electrostatic (red lines) potentials with interparticle distance $d$ calculated for $[NaCl] = 5 \cdot 10^{-3} M$ (long-dash) and their sum (grey line). The electrostatic potential for $[NaCl] = 150 \cdot 10^{-3} M$ is also shown (short-dash). (For interpretation of the references to color in this figure caption, the reader is referred to the web version of this paper.)



**Fig. 2.** Measured solvent phase diagram showing the dependence of the phase separation temperature on the composition of the solvent mixture, for three different concentrations of NaCl: 0 ( □ ), 5 ( ● ) and 150 ( ◆ ) $10^{-3}$ M.

In the case presented here, the binary mixture shows an inverted miscibility gap: the two solvent components phase separate into coexisting liquids at high temperatures, and become homogeneously mixed at rather low temperatures. In the homogeneous phase, but close to the phase separation line, solvent-mediated attractive interactions arise between suspended particles. A particular well-controlled and universal interaction occurs close to the critical point of the solvent, which terminates the miscibility gap, see the red dot in Fig. 1. Close to the critical point, solvent concentration fluctuations become long range, and their confinement between particle surfaces gives rise to so-called critical Casimir forces: In analogy to the quantum mechanical Casimir effect, in which confinement of zero-point fluctuations of the electromagnetic field between two conductive walls gives rise to an attractive force [16], the confinement of solvent fluctuations in the liquid gap between immersed surfaces gives rise to attractive critical Casimir forces [15,17–21]. While approaching the solvent phase separation temperature $T_s$ with $\Delta T = |T_s - T|$ decreasing, the length scale of the fluctuations, $\xi$, increases. An attractive force between two particles separated by a distance $d$ arises when $\xi$ becomes of the same order as $d$. The value of $\xi$ rises upon approaching the critical point, where it diverges [22].

The wetting properties of the colloidal particles set the boundary conditions of the critical Casimir effect: depending on the surface chemistry (charge, passivation layer), the particle surfaces are wet either by the 3MP-rich or water-rich phase. This has important consequences on the aggregation of the particles. In fact, when on the left side of the critical composition the fluctuating regions are 3MP-rich, and vice versa on the right side, as shown in Fig. 1. Therefore, colloids featuring hydrophilic surfaces, such as the QDs used in this work, very weakly aggregate on the left side, as they are not wet and only weakly confine fluctuations. Conversely, strong aggregation is observed on the right side.
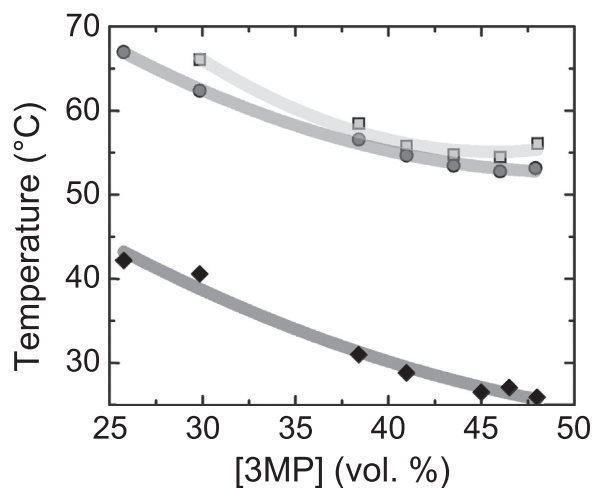
QDs in this regard are quite a unique case, their radius $r$ is of the order of a few nanometers and therefore generally smaller than $\xi$ in any range of $\Delta T$ achieved in this system. This is a completely different regime from what has been investigated in the literature, where the minimum particle size studied is $r = 50$ nm [23].

The unique feature of the critical Casimir effect to achieve colloidal particle assembly is its reversibility. Unlike salt-induced aggregation by Van der Waals forces, it should be possible to completely eliminate the attractive critical Casimir force by increasing $\Delta T$ and therefore the distance to the critical point. The number of fluctuations per unit volume decreases and $\xi$ shrinks below $d$. This feature should provide an exquisitely sensitive temperature-dependent knob that controls the aggregation of the dispersion.

The hydrophilic QDs used in this work are charge-stabilized in pure water, exhibiting a Coulombic repulsive potential. The magnitude of the interparticle electrostatic repulsion can be tuned by adding NaCl in solution, this decreases the Debye screening length $\ell_D$. For high enough NaCl content, $[NaCl] = 150 \cdot 10^{-3} M$, we observe indeed that the QDs precipitate. This is an example of the "salting out" effect, as the electrostatic repulsion length scale drops and the nanoparticles become attractive due to Van der Waals forces. By contrast, the dots are stable for several months at the much lower salt concentration $5 \cdot 10^{-3} M$, the concentration used in the remainder of this work. Nevertheless, in binary mixtures with [3MP] $\leq$ 46% with $5 \cdot 10^{-3} M$ NaCl, aggregation takes place when tuning $\Delta T$ to increase $\xi$. By controlling $\ell_D([NaCl])$, $\xi(\Delta T)$, and [3MP], we are able to study the assembly in response to the effective potential: the sum of repulsive and attractive contributions as represented by the inset of Fig. 2 [18,19].

## 3. Materials and methods

### 3.1. Binary mixture water-3MP

We use a binary mixture of 3-methylpyridine (3MP) and water, this binary mixture alone does not show a phase separation temperature [22,24]. However, upon addition of a third component such as NaCl and/or QDs, the mixture phase separates above a certain temperature $T_s$ as shown in Fig. 1. The two phases are differently composed: the top lighter phase is richer in 3MP, while the bottom heavier one is predominantly composed of water. We explored a range of compositions with 3MP volume fraction

between 26 and 48%. For the dynamic light scattering measurements presented below, we focused on a sample on the *left side* composed of $[3MP] = 43.5 \; vol\%$ and a sample on the *right side* containing $[3MP] = 48.0 \; vol\%$.

### 3.2. Quantum dots synthesis

Cadmium Telluride QDs were synthesized according to published methods [25]. Here, the synthesis used sodium borohydride ($NaBH_4$) as the reducing agent, thioglycolic acid as the stabilizing ligand, and cadmium acetate ($Cd(OCOCH_3)$) and potassium telluride ($K_2TeO_3$) as inorganic sources with molar ratios of 1.0 : 1.0 : 0.2 of ligand : $Cd^{2+}$ : $TeO_3^{2-}$. During the formation of the QDs, the ligand partially decomposed forming $S^{2-}$ and reacted with $Cd^{2+}$ to form CdS, which provided a stabilizing shell and increased quantum yield. After synthesis, the QDs are dispersed in water and used without further purification.

### 3.3. Sample preparation

Deionized water was obtained from a Milli−Q® Integral Water Purification System (Merck Millipore) and filtered through a 25 nm mixed cellulose membrane (Merck Millipore). 3MP (Sigma Aldrich, ≥ 99.5%) was distilled and filtered through a 100 nm PTFE membrane (Merck Millipore).

Binary mixture samples were prepared by mixing the different components in a 0.5 mL tube; when needed, we added NaCl as a 1 M solution in water. The final volume was typically 250 μ L. We transferred the mixture to a NMR tube which we flame sealed, while keeping the solution in the vessel cold to minimize heating and evaporation. The flame sealed tube containing the final mixture was immediately used to measure $T_s$ or inserted in the dynamic light scattering setup. A new sample was prepared for each measurement.

We found that the concentration of QDs has an influence on the binary solvent phase diagram affecting the value of $T_s$; we thus kept a constant QD concentration throughout all experiments. This result is not surprising as experimental evidence shows that altering the water and heavy water content in such a mixture can cause the value of $T_s$ to shift by several tens of degrees due to the different hydrogen bonding contribution [24]. We speculate that unbound ligands present in the QD dispersion may indeed play a role in this respect, although it is not yet clear what is the underlying mechanism causing this shift. Other more strongly bound ligands, such as lipoic acid [26], may indeed be more suited for working in 3MP mixtures as 3MP itself may undergo surface ligand exchange. However, as QDs appear completely stable in binary mixtures for several months such an exchange process, which would yield hydrophobic QDs, is likely slow.

### 3.4. Determination of $T_s$

We first study the phase separation of the solvent. We experimentally determined the phase-separation temperature of the binary solvent containing the QDs. We used a thermostated water bath with temperature control of 0.05 °C and heated the prepared mixture, stored in a flame sealed NMR tube, until opalescence was detected and the sample turned turbid. Such an effect is due to the onset of phase separation, namely the formation of light-scattering droplets, allowing us to pinpoint phase separation precisely.

### 3.5. Dynamic light scattering

We then use dynamic light scattering to follow the aggregation of quantum dots with time. Dynamic light scattering (DLS) is a well-established method to determine the hydrodynamic radius of suspended objects. In a classical picture, when coherent light impinges upon a region of refractive index mismatch compared to the surrounding solvent, scattering is observed. Scattered light from suspended particles shows constructive or destructive interference depending on the phase difference between the scattered waves; this depends on the difference in optical path of the scattered wavefronts, and therefore on the relative positions of the scattering objects. As the particles undergo Brownian motion, the interference pattern changes. DLS measures the time decay of typical fluctuations in the interference pattern and relates it to the Brownian motion of the scatterers. This is done by correlating the scattered light intensity between different delay times $\tau$ from which an intensity correlation function $g_2(\tau) - 1$ is constructed. For a monodisperse sample, the intensity correlation function decays as a single exponential with decay time $\tau_c$ that is proportional to the hydrodynamic radius of the scattering objects according to $R_H = (kT/6\pi\eta)q^2\tau_c$ where $k$ is Boltzmann's constant, $T$ the temperature, $\eta$ the solvent viscosity and $q = (4\pi n/\lambda)\sin(\theta/2)$ the scattering vector; for all measurements, the scattering angle $\theta$ and the refractive index $n$ are kept constant [27].

In this work, a typical DLS run was 60 s long; scattered photons reaching the two photodetectors were cross-correlated to give one intensity correlation function per measurement. We use a ALV DLS setup featuring a digital correlator and a $\lambda = 633$ nm HeNe laser (35 mW) to minimize fluorescence. By using a water circulator system, we ensure a temperature stability of the chamber of the order of $\pm 0.01°C$. We let the chamber equilibrate at the desired working temperature for $\sim 0.5$ h, and then insert the tube filled with the QD dispersion. For each measurement, we discarded the first 5 minutes, during which the scattering intensity changes due to heating or cooling of the sample to the desired working temperature. Finally, due to the different size of solvent fluctuations, intensity values were normalized by the initial signal to account for different relative intensities between samples and thus allow a meaningful comparison.

## 4. Results and discussion

The measured phase diagram of the binary mixture with quantum dots is shown in Fig. 2, where we plot the phase-separation temperature as a function of 3MP concentration. Three different phase lines reveal a clear dependence on the NaCl concentration in the mixture. We can estimate the critical composition from the minimum of the diagram shown in Fig. 2 [24]. Taking the phase lines for NaCl content of 0 M ( ☐ ) and $5 \cdot 10^{-3} M$ ( ● ), we estimate the critical composition to be $[3MP]_c \simeq 45.75 \; vol\%$. Based on the knowledge that particles are preferentially wet by one fluctuation composition, we have prepared mixtures on the left and right side of this critical composition to test the effect of wetting.

Using a binary solvent on the left side of the critical point, we can readily observe temperature-dependent QD aggregation by eye as shown in Fig. 3. While a QD dispersion at $\Delta T = 20°C$ is stable, showing a homogeneous image intensity, by contrast at $\Delta T = 1°C$ the coarsening of image intensity suggests QD aggregation. Emerging spots that scatter the illuminating light indicate QD aggregates that grow in size. To investigate this aggregation in more detail, we use dynamic light scattering to measure the size of the growing QD aggregates as a function of time.

On the left side of the critical composition, the temperature clearly controls the aggregation process in agreement with the visual observations in Fig. 3. The aggregation of quantum dots is reflected in the intensity magnitude and correlation function of the scattered light as shown in Fig. 4: both evolve differently with time depending on $\Delta T$. When far from phase separation ( ● ,
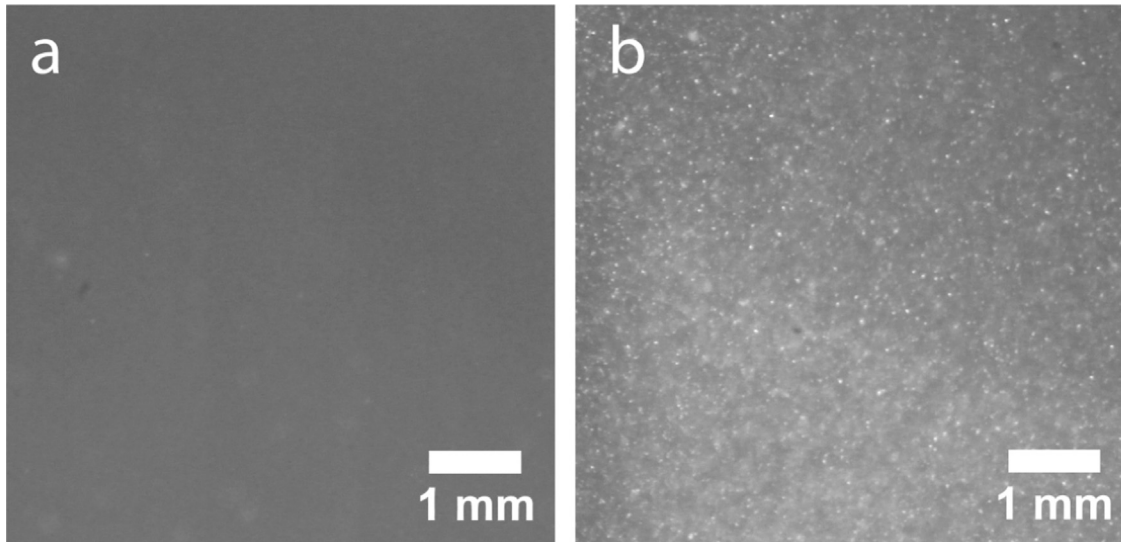
**Fig. 3.** Visual impression of quantum dot assembly in binary liquid solvents. Photographs of the scattered light reveal uniform dispersions (a) and dispersions with aggregates (b). (a) Far from the separation temperature (ΔT=20°C), the particles remain suspended and the image looks uniform. (b) Close to the phase separation temperature (ΔT=1°C), the quantum dots aggregate and flocks of scattered light appear. Pictures were taken 24 h after sample preparation.
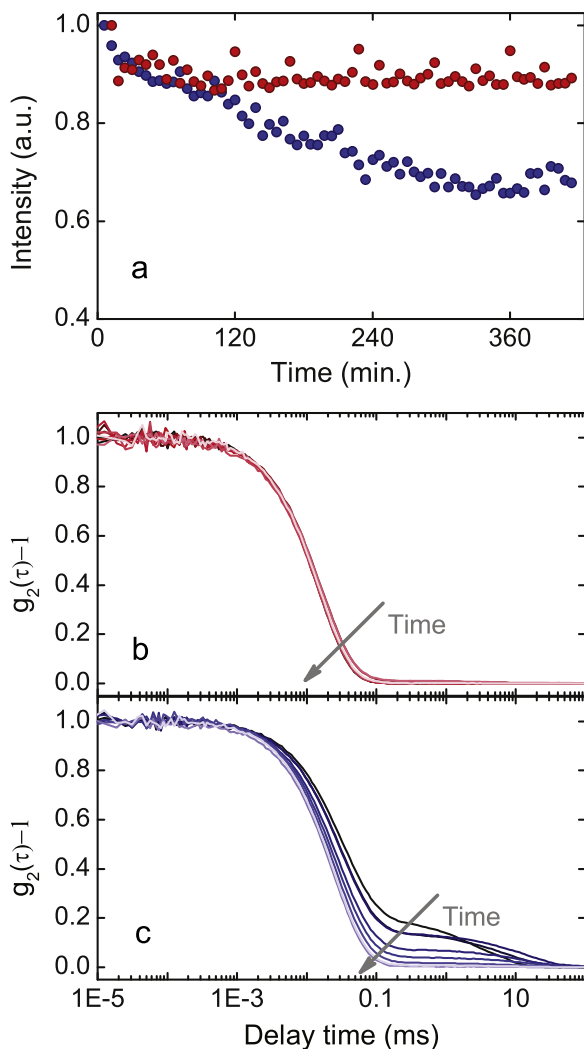


**Fig. 4.** Dynamic light scattering of quantum dot suspensions on the left side of the critical point. (a) Scattering intensity as a function of time at ΔT=20°C ( 🔴 ) and 1°C ( 🔵 ). (b,c) Time evolution of the intensity correlation function at ΔT=20°C (b) and 1 °C. (c) Measurements were taken every hour (dark to light colour).

ΔT=20°C), the intensity is quite stable, dropping down only by < 10%, which indicates that particles remain suspended, as shown in Fig. 4a. The correlation functions nearly perfectly overlap with one another, showing a single exponential decay with decay time $\tau_c$ corresponding to scattering objects with size 2.6 nm, as shown in Fig. 4b. This value is indeed consistent with the hydrodynamic radius of the QDs in pure water. Additionally, the solvent fluctuations scatter light and give rise to an additional decay in the correlation function, which is fixed for a constant $\Delta T$. Since we are not able to discern two distinct decays in the correlation function, we conclude that the correlation length of the solvent fluctuations is of the same order as that of the QDs, but still the solvent fluctuations are too weak to induce particle aggregation.

The situation appears completely different when close to $T_s$ ( 🔵 , ΔT=1°C). The intensity drops by ∼ 30%, and the correlation curve immediately shows a double decay, the second decay growing in time. Our interpretation is the following: Due to the proximity to the critical point, solvent fluctuations become significant and cause critical Casimir forces that lead to particle aggregation. This appears as two decays, the first one representing the solvent fluctuations, and the second one representing the growing aggregates, whose growth is reflected in the shift of the second decay to longer times. Interestingly, the second decay drops in magnitude and disappears completely by the end of the observation time, 7 h, indicating that the aggregates sediment to the bottom of the tube, hence escaping from the field of view. This is reasonable, given the high density mismatch between CdTe particles and binary mixture, $\Delta\rho \sim 4.8\ \mathrm{g\,cm^{-3}}$. From the time constant of the diminishing second decay, we determine that the aggregates reach an average radius of ∼ 700 nm. We can estimate the maximum size of aggregates that remain suspended from the balance of the Stokes sedimentation velocity, $U_0$ and the diffusion coefficient, $D_0$. The ratio of the two defines the dimensionless Péclet number, $Pe = (2aU_0)/D_0$, where $a$ is the average aggregate size, $U_0 = (2a^3\Delta\rho g)/9\eta$ and $g$ is the gravitational acceleration. Assuming a value of $Pe=1$, which approximates sedimentation equal to diffusion, the calculated $a(Pe=1) \sim 375$ nm corresponds well to the measured value of $a \sim 700$ nm. Therefore the apparent size to which the aggregates grow should be taken more as an order of magnitude.
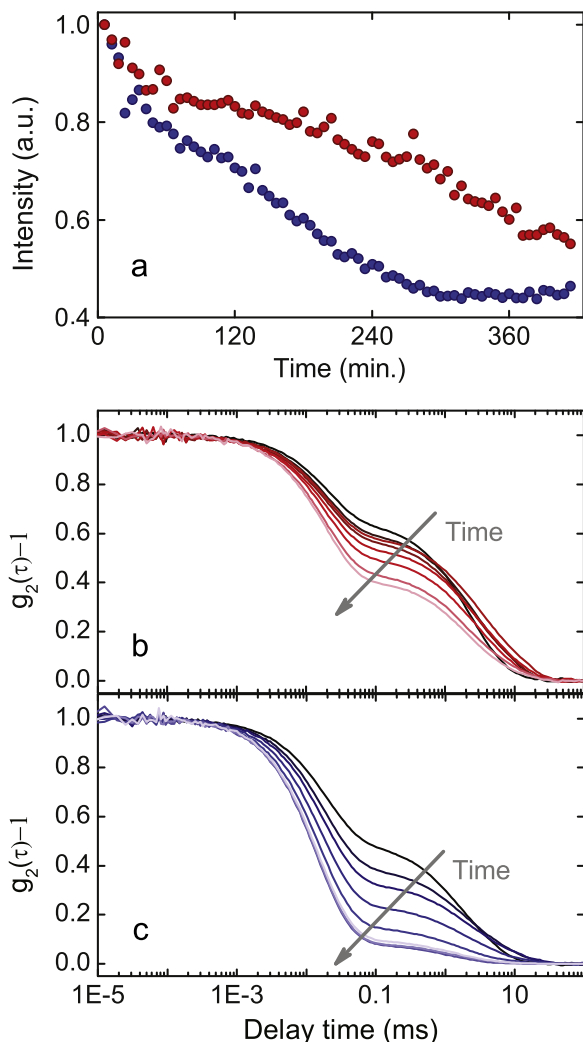
**Fig. 5.** Dynamic light scattering of quantum dot suspensions on the right side of the critical point. (a) Scattering intensity as a function of time at $\Delta T = 20°C$ ( 🔴 ) and $1°C$ ( 🔵 ). (b,c) Time evolution of the intensity correlation function at $\Delta T = 20°C$ (b) and $1°C$. (c) Measurements were taken every hour (dark to light colour).

To explore the full aggregation behavior in binary mixtures, we also use solvent compositions on the other side of the critical point. From the literature, it is known that for compositions poor in the component preferred by the particles, corresponding in our case to compositions on the right side of the critical point, much larger critical Casimir forces occur [28,29]. Indeed, on the right side of the critical composition, the scattered light intensity shows a much faster drop in the signal by $\sim 50\%$ even at $\Delta T = 20°C$ and the correlation functions show growing aggregates. This is again reflected in the second decay evolving with time and decreasing in magnitude; in contrast to the behavior on the left side of the critical composition at the same $\Delta T = 20°C$, where no aggregation was observed. Yet, the fact that the second decay does not vanish completely at the end of the observation time (cf. Fig. 4c) indicates that the aggregation process is slower, and the resulting aggregates have a smaller $Pe$ and remain suspended for longer time.

When subjecting a sample of identical composition to a smaller $\Delta T = 1°C$, the relative scattering intensity signal drops faster and by a larger extent; the correlation functions show that the second decay drops strongly in magnitude as aggregates sediment faster. Visual inspection of the tube shows that indeed nearly all of the QDs flocculated to the bottom and the solution looks clear. After

leaving the vial at room temperature, $\Delta T \approx 35°C$, for a few hours, the sediment redisperses into solution. We interpret this observation as reversibility of the assembly: for sufficiently large $\Delta T$, i.e. sufficiently far away from the solvent critical point, the attractive force becomes negligible and particle resuspension is mediated by the electrostatic repulsion. These results thus demonstrate a new, reversible way to assemble QDs with temperature as control parameter. To quantify the extent of the redispersion, further investigation is required Fig. 5.

The assembly of QDs over a large temperature interval as much as 20°C below the critical point is remarkable. It demonstrates the importance of critical Casimir forces for nano-scale objects. As shown by DLS, QDs have a strong tendency to aggregate in solvents close to their phase separation temperature, on the left side of the critical point as well as on the right side, where assembly happens on an even shorter time scale. In contrast, no assembly is observed on the non-wetting side when far from $T_s$, in line with recent work on micron-scale colloidal systems [20]. It is interesting that we see assembly in our nanometer-scale QDs at all, as the solvent correlation length is of the same order, or even larger than the particles themselves; this is a "reversed" length scale regime to what has been studied so far, where the particles were always larger than the solvent correlation length. The fact that assembly on the wetting side takes place at larger $\Delta T$ compared to micron-scale colloids is likely related to these inverted length scale conditions, which we have investigated in this work.

## 5. Conclusions

We report reversible assembly of quantum dots via critical Casimir forces. Mastering critical Casimir forces on the nanoscale could provide a pioneering approach for reversible, programmed, ordered assembly of nanoparticles and enable the study of growth kinetics of superstructures as condensation takes place in solution. Importantly, the use of this technique could allow the temperature-controlled growth of quantum-dot superstructures as bottom-up technique for new optoelectronic materials. The results are particularly significant as they take place at the crossroad between nanotechnology, colloidal, and material science, and promote the successful interplay among these fields. This new method opens an opportunity to assemble structures by design, tuning key parameters such as the interparticle distances by the exquisite temperature control over the critical Casimir interactions.

## References

[1] A. Dong, J. Chen, P.M. Vora, J.M. Kikkawa, C.B. Murray, Binary nanocrystal superlattice membranes self-assembled at the liquid–air interface, Nature 466 (7305) (2010) 474–477.
[2] M. Boneschanscher, W. Evers, J. Geuchies, T. Altantzis, B. Goris, F. Rabouw, S. van Rossum, H. van der Zant, L. Siebbeles, G.Van. Tendeloo, et al., Long-range orientation and atomic attachment of nanocrystals in 2D honeycomb superlattices, Science 344 (6190) (2014) 1377–1380.
[3] M. Cargnello, A.C. Johnston-Peck, B.T. Diroll, E. Wong, B. Datta, D. Damodhar, V.V. Doan-Nguyen, A.A. Herzing, C.R. Kagan, C.B. Murray, Substitutional doping in nanocrystal superlattices, Nature 524 (7566) (2015) 450–453.
[4] D. Vanmaekelbergh, Self-assembly of colloidal nanocrystals as route to novel classes of nanostructured materials, Nano Today 6 (4) (2011) 419–437.

[5] M.V. Kovalenko, L. Manna, A. Cabot, Z. Hens, D.V. Talapin, C.R. Kagan, V.I. Klimov, A.L. Rogach, P. Reiss, D.J. Milliron, et al., Prospects of nanoscience with nanocrystals, ACS nano 9 (2) (2015) 1012–1057.

[6] M.V. Kovalenko, M. Scheele, D.V. Talapin, Colloidal nanocrystals with molecular metal chalcogenide surface ligands, Science 324 (5933) (2009) 1417–1420.

[7] A.T. Fafarman, W.-k. Koh, B.T. Diroll, D.K. Kim, D.-K. Ko, S.J. Oh, X. Ye, V. Doan-Nguyen, M.R. Crump, D.C. Reifsnyder, et al., Thiocyanate-capped nanocrystal colloids: vibrational reporter of surface chemistry and solution-based route to enhanced coupling in nanocrystal solids, J. Am. Chem. Soc. 133 (39) (2011) 15753–15761.

[8] I.-H. Chu, M. Radulaski, N. Vukmirovic, H.-P. Cheng, L.-W. Wang, Charge transport in a quantum dot supercrystal, J. Phys. Chem. C 115 (43) (2011) 21409–21415.

[9] J.-H. Choi, A.T. Fafarman, S.J. Oh, D.-K. Ko, D.K. Kim, B.T. Diroll, S. Muramoto, J.G. Gillen, C.B. Murray, C.R. Kagan, Bandlike transport in strongly coupled and doped quantum dot solids: a route to high-performance thin-film electronics, Nano Lett. 12 (5) (2012) 2631–2638.

[10] C.R. Kagan, C.B. Murray, Charge transport in strongly coupled quantum dot solids, Nat. Nanotechnol. 10 (2015) 1013–1026.

[11] D. Vanmaekelbergh, P. Liljeroth, Electron-conducting quantum dot solids: novel materials based on colloidal semiconductor nanocrystals, Chem. Soc. Rev. 34 (4) (2005) 299–312.

[12] T. Hanrath, Colloidal nanocrystal quantum dot assemblies as artificial solids, J. Vac. Sci. Technol. A 30 (3) (2012) 030802.

[13] W.J. Baumgardner, K. Whitham, T. Hanrath, Confined-but-connected quantum solids via controlled ligand displacement, Nano Lett. 13 (7) (2013) 3225–3231.

[14] S. Kondrat, L. Harnau, S. Dietrich, Critical Casimir interaction of ellipsoidal colloids with a planar wall, J. Chem. Phys. 131 (20) (2009) 204902.

[15] C. Hertlein, L. Helden, A. Gambassi, S. Dietrich, C. Bechinger, Direct measurement of critical Casimir forces, Nature 451 (7175) (2008) 172–175.

[16] HB. Casimir, On the attraction between two perfectly conducting plates, In: Proceedings of K. Ned. Akad. Wet, vol. 51, 150, 1948.

[17] M.E. Fisher, P.-G. de Gennes, Phenomenes aux parois dans un melange binaire critique, CR Acad. Sci. Ser. B 287 (1978) 207–209.

[18] D. Bonn, J. Otwinowski, S. Sacanna, H. Guo, G. Wegdam, P. Schall, Direct observation of colloidal aggregation by critical Casimir forces, Phys. Rev. Lett. 103 (15) (2009) 156101.

[19] S.J. Veen, O. Antoniuk, B. Weber, M.A. Potenza, S. Mazzoni, P. Schall, G.H. Wegdam, Colloidal aggregation in microgravity by critical Casimir forces, Phys. Rev. Lett. 109 (24) (2012) 248302.

[20] V.D. Nguyen, S. Faber, Z. Hu, G.H. Wegdam, P. Schall, Controlling colloidal phase transitions with critical Casimir forces, Nat. Commun. 4 (2013) 1584.

[21] P.B. Shelke, V. Nguyen, A. Limaye, P. Schall, Controlling colloidal morphologies by critical Casimir forces, Adv. Mater. 25 (10) (2013) 1499–1503.

[22] T. Narayanan, A. Kumar, Reentrant phase transitions in multicomponent liquid mixtures, Phys. Rep. 249 (3) (1994) 135–218.

[23] H. Guo, T. Narayanan, M. Sztuchi, P. Schall, G.H. Wegdam, Reversible phase transition of colloids in a binary liquid solvent, Phys. Rev. Lett. 100 (18) (2008) 188303.

[24] J. Cox, Phase relationships in the pyridine series Part II. The miscibility of some pyridine homologues with deuterium oxide, J. Chem. Soc. (1952) 4606–4608.

[25] S. Wu, J. Dou, J. Zhang, S. Zhang, A simple and economical one-pot method to synthesize high-quality water soluble CdTe QDs, J. Mater. Chem. 22 (29) (2012) 14573.

[26] G. Palui, T. Avellini, N. Zhan, F. Pan, D. Gray, I. Alabugin, H. Mattoussi, Photo-induced phase transfer of luminescent quantum dots to polar and aqueous media, J. Am. Chem. Soc. 134 (39) (2012) 16370–16378.

[27] C.S. Johnson, D.A. Gabriel, Laser light scattering, Spectr. Biochem. 2 (1981) 177–272.

[28] A. Gambassi, A. Maciołek, C. Hertlein, U. Nellen, L. Helden, C. Bechinger, S. Dietrich, Critical Casimir effect in classical binary liquid mixtures, Phys. Rev. E 80 (6) (2009) 061143.

[29] T.F. Mohry, S. Kondrat, A. Maciołek, S. Dietrich, Critical Casimir interactions around the consolute point of a binary solvent, Soft Matter 10 (30) (2014) 5510–5522.